NKX2-1 (TTF-1) gene re-expression induces cell death through apoptosis and necrosis in dedifferentiated thyroid carcinoma cells

学　位　論　文

NKX2-1 re-expression induces cell death through apoptosis and necrosis in dedifferentiated thyroid carcinoma cells

（NKX2-1 再発現によるアポトーシスとネクローシスを介した
脱分化甲状腺癌細胞の細胞死誘導効果）

福島県立医科大学大学院医学研究科

検査医科学

伊藤 祐子

概要

【背景・目的】

一般的に甲状腺癌は予後良好な疾患とされる。しかし、一部は低分化癌や未分化癌であり、治療抵抗性で短期間に局所浸潤・他臓器転移を来すため予後は極めて不良である。このような脱分化甲状腺癌においては、甲状腺特異的転写因子（thyroid transcription factor; TTF）の発現が低下していることが報告されている。TTF には、NK2 homeobox 1（NKX2-1：TTF-1 と同一）、forkhead box E1（FOXE1：TTF-2 と同一）、paired box 8（PAX8）、hematopoietically expressed homeobox（HHEX）があり、それらは甲状腺の形態形成や機能維持に重要な役割を果たす。甲状腺ホルモン合成に関連するサイログロブリン遺伝子、甲状腺ペルオキシダーゼ遺伝子、TSH 受容体遺伝子などは TTF によって調節されるため、TTF 非発現脱分化甲状腺癌においては、これらの甲状腺特異的遺伝子の発現も低下あるいは消失している。我々のグループはこれまで、NKX2-1 非発現甲状腺癌細胞に *NKX2-1* 遺伝子を導入することにより、失われていたサイログロブリン遺伝子、甲状腺ペルオキシダーゼ遺伝子の再発現を誘導し、取り込まれた放射性ヨウ素の有機化および細胞内保持をもたらすことを報告した。その一方、*NKX2-1* 遺伝子導入により細胞死が誘導されることを観察した。NKX2-1 は甲状腺以外に肺にも発現しているが、肺癌において *NKX2-1* は、癌細胞の生存にその発現維持が必要な lineage-survival oncogene であると同時に、浸潤・転移・進展の抑制に関与し、相反する二面性があることが報告されている。

脱分化甲状腺癌における細胞死誘導機序の解明は、上述のような低分化および未分化甲状腺癌の新たな治療戦略に繋がることが期待される。本研究では、NKX2-1 非発現脱分化甲状腺癌において、*NKX2-1* 遺伝子導入により観察された細胞死誘導効果について詳細に検討した。さらに、その機序を解明するため NKX2-1 再発現により誘導された遺伝子発現量の変化を網羅的に解析し、顕著な増加を示した遺伝子について細胞死への関与を検討した。

【方法】

甲状腺乳頭癌患者組織由来の、*NKX2-1* 遺伝子発現が消失している細胞株 BHP18-21v（NKX2-1^{-}/PAX8^{+}）を用いた。*NKX2-1* 遺伝子導入にはラット *Nkx2-1* 発現アデノウイルスベクター（AdTTF-1）を用い、コントロールとして *LacZ* 発現アデノウイルスベクター（AdLacZ）を用いた。まず、一定時間後に生細胞量の測定、アポトーシスおよびネクローシスの有無を調べた。生細胞定量に CCK-8 を用いた。アポトーシスおよびネクローシスの検出はアクリジンオレンジ・エチジウムブロミド二重染色、Hoechst 33342

染色、アガロースゲル電気泳動、およびアネキシン V によるリアルタイムアッセイの 4 法で行った。次に、GeneChip によりアデノウイルスベクター感染後の遺伝子発現量を網羅的に解析し、コントロールに対し増加が大きい遺伝子を選択し real-time PCR によりその発現量を測定した。さらに、遺伝子発現量が著増した遺伝子に対する siRNA（siARG2、siRGS4、siRGS5）を導入し、それぞれの遺伝子発現を抑制した細胞において、AdTTF-1 感染後の生細胞、アポトーシスおよびネクローシスを検出し、コントロール siRNA（siNegative）と比較した。

【結果】

AdLacZ に対し、AdTTF-1 感染細胞において時間依存性、ウイルスの multiplicity of infection (MOI)依存性に生細胞は有意に減少し、細胞死誘導を認めた。同じく甲状腺乳頭癌由来である BHP7-13 細胞（NKX2-1$^-$/PAX8$^+$）においても有意な細胞死誘導を認めたが、イヌ腎由来 MDCK 細胞（NKX2-1$^-$/PAX8$^+$）とヒト肝細胞癌由来 HepG2 細胞（NKX2-1$^-$/PAX8$^-$）においては AdTTF-1 感染による有意な細胞死を認めず、甲状腺癌特異的であった。アクリジンオレンジ・エチジウムブロミド二重染色、Hoechst 33342 染色、アガロースゲル電気泳動，およびリアルタイムアッセイの結果、いずれの方法も AdTTF-1 感染細胞においてアポトーシスとネクローシスの両者が検出された。GeneChip 解析にて、arginase 2（*ARG2*）、regulator of G protein signaling 4（*RGS4*）および *RGS5* は、AdLacZ に比し AdTTF-1 感染細胞において顕著な増加を認めた。これらの遺伝子発現量を real-time PCR で測定した結果、*ARG2* は非感染細胞に比し最大 23.5±1.2 倍、*RGS4* は 129.8±39.7 倍、*RGS5* は 550.2±191.8 倍に増加した。siRNA 導入により、AdTTF-1 感染後の生細胞は siARG2 導入細胞で siNegative に対し 115.7±2.7%、siRGS4 導入細胞で 113.2±4.2%に増加し、細胞死が抑制された。siRGS5 導入細胞では有意な変化を認めなかった。また、siARG2 および siRGS4 導入細胞においてアポトーシスは siNegative に対しそれぞれ 82.4±3.7%および 71.5±5.4%に、ネクローシスはそれぞれ 78.7±6.1%および 62.3±8.6%に抑制された。ARG2 と RGS4 は *NKX2-1* 遺伝子導入による BHP18-21v 細胞の細胞死、アポトーシスおよびネクローシス誘導に関与することが示された。

【考察】

NKX2-1 とアポトーシスとの関連については、肺癌において NKX2-1 が腫瘍抑制やアポトーシス促進作用を有する可能性のあることが報告されている。本研究においてはネクローシスも同時に検出された。遺伝子によって調節されたネクローシス はネクロトーシスと言われており、本研究における *Nkx2-1* 遺伝子導入に誘導されたネクローシスは

ネクロトーシスである可能性も示唆された。

ARG2 はアルギニンの代謝酵素である。アルギニンは多くの細胞内代謝やシグナル伝達などに重要な役割を果たし、特にポリアミンや一酸化窒素の基質となることから、アルギニンを減少させることが癌の治療の１つとして試みられている。RGS は G 蛋白を介し細胞や臓器の生理機能を多様な側面から調節する。ARG2 および RGS4 発現と癌との関連は様々な組織において報告されている。しかし、それらの発現が癌細胞の増殖、浸潤、転移を抑制しアポトーシスを促すという報告がある一方、逆の報告も多数ある。癌細胞の特徴、臓器の違い、癌の進行度などにより効果が異なると考えられる。

肺癌に関しては、ホメオボックス遺伝子である *DLX4* を欠失した高転移性の肺癌細胞に *DLX4* を強制発現させた結果、in vitro および in vivo において癌の抑制効果を認めたことが報告されている。本研究結果は、脱分化甲状腺癌細胞に失われた *NKX2-1* 遺伝子を再発現させることが癌の進展抑制に効果をもたらし得ることを示唆している。

【結語】

Nkx2-1 遺伝子導入により、アポトーシスおよびネクローシスの両者を介して NKX2-1 非発現脱分化甲状腺癌細胞の細胞死が誘導された。また、*ARG2* 遺伝子と *RGS4* 遺伝子が NKX2-1 再発現によるアポトーシスおよびネクローシスに関与している可能性が示唆された。

Contents

Abbreviations

AdLacZ	adenoviral vector containing *LacZ*
ADT	arginine deprivation therapy
AdTTF-1	adenoviral vector containing *Nkx2-1*
ARG2	arginase 2
CCK-8	Cell Counting Kit-8
CMV	cytomegalovirus
DLX4	distal-less homeobox 4
DMEM	Dulbecco's modified Eagle medium
EDTA	ethylenediaminetetraacetic acid
FBS	fetal bovine serum
FOXE1	forkhead box E1
GAPDH	glyceraldehyde-3-phosphate dehydrogenase
HDAC	histone deacetylase
HHEX	hematopoietically expressed homeobox
MAPK	mitogen-activated protein kinase
MOI	multiplicity of infection
NIS	sodium iodide symporter
NKX2-1	NK2 homeobox 1
NO	nitric oxide
PAX8	paired box 8
PBS	phosphate-buffered saline
PCR	polymerase chain reaction
RGS	regulator of G protein signaling
RIPK	receptor-interacting protein kinase
SEM	standard error of the mean
TG	thyroglobulin
TNF	tumor necrosis factor
TPO	thyroid peroxidase
TSHR	thyroid stimulating hormone receptor
TTF	thyroid transcription factor
UNG	uracil-N-glycosylase

Introduction

The thyroid transcription factors (TTFs) are fundamental to proper formation of the thyroid gland and for maintaining the functional differentiated state of the adult thyroid (1). NK2 homeobox 1 (NKX2-1), also known as thyroid transcription factor 1 (TTF-1), forkhead box E1 (FOXE1), paired box 8 (PAX8) and hematopoietically expressed homeobox (HHEX) are known as the TTFs. The roles of NKX2-1, FOXE1, and PAX8 are to bind to DNA and to regulate thyroid specific genes that drive thyroid hormone synthesis, such as thyroglobulin (*TG*), thyroid peroxidase (*TPO*), thyroid stimulating hormone receptor (*TSHR*), and the sodium iodide symporter (*NIS,* also known as solute carrier family 5 member 5). Simultaneous expression of the four TTFs is unique to thyroid follicular cells, although each of the TTFs is expressed in several other tissues in adult humans; NKX2-1 is expressed in the lung and nervous system, and FOXE1 and PAX8 are expressed in a number of tissues (1).

Since both cell proliferation and differentiation are involved in the process of normal development and cancer development, it has been suggested that the genes critical for development act on tumorigenesis in various tissues where they are expressed, including the thyroid (2). There are several reports describing the associations between TTFs expressions and carcinogenesis in non-thyroid tissues, as well as in thyroid glands. PAX8 expressions have been reported to be increased in neoplastic renal tissues (3), Wilms tumor (4), Müllerian carcinoma (5) and ovarian cancer (6). Regarding the lungs, NKX2-1 is required for the maintenance of physiological lung functions in addition to its developmental roles. In lung adenocarcinoma, NKX2-1 expression was increased (7) and conferred a better prognosis (8). Kusakabe *et al*. reported that conditional knockout of *Nkx2-1* in mice resulted in thyroids with very disorganized structure and the follicular

cells undergoing degeneration (9). Consequently, their thyroids had approximately a 2-fold higher proliferation rate, which contributed to a higher incidence of thyroid tumors induced by genotoxic carcinogen (10).

As concerning dedifferentiation in thyroid cancer, the model of multi-step carcinogenesis has been proposed based on general concepts and specific pathways (11). Genomic instabilities induced by risk factors result in early genetic alterations that involve the mitogen-activated protein kinase (MAPK) signaling pathway. Oncogenic activation of MAPK signaling leads to later genetic alterations that involve other signaling pathways, cell-cycle regulators and various adhesion molecules. Accelerating the interactions between genomic instability and genetic alterations promotes progression from well-differentiated to undifferentiated thyroid carcinoma (11). In thyroid cancer, an immunohistochemical analysis showed that NKX2-1 expressions decreased corresponding to the progressive dedifferentiation of thyroid tumors (12). Dedifferentiated thyroid cancers are commonly defined as differentiated or poorly differentiated thyroid cancers which, during tumor progression, lose their ability to uptake and concentrate radioiodine, and in some cases to produce thyroglobulin (13). Ros *et al.* reported that the expression of thyroid specific genes, such as *TG*, *TPO*, and *TSHR*, were decreased or lost in dedifferentiated thyroid cancers in which *NKX2-1* and *PAX8* gene expressions were absent (14). We have previously reported that both TG and TPO mRNA and their protein levels were re-expressed in dedifferentiated thyroid cancer cells ($NKX2\text{-}1^{-}/PAX8^{+}$) when these cells were infected with adenoviral vectors containing *Nkx2-1* (AdTTF-1), which induced radioiodide organification and retention in those cells (15).

Yamaguchi *et al.* described that *NKX2-1* played a role as a lineage-survival oncogene in lung adenocarcinomas, whereas it also inhibited invasion, metastasis, and progression, paradoxically conferring better prognosis (16). Similarly, while we demonstrated the re-expression of TG and

TPO in dedifferentiated thyroid cancer cells by transduction of *Nkx2-1* (15), we coincidentally observed cell death in those cells. The observations in the NKX2-1-re-expressed thyroid cancer cells suggested that NKX2-1 has a role as suppressor for progression of thyroid cancer cell, as well as a role for maintaining the function of normal thyroid follicular cells. However, the molecular pathways and mechanisms that connect TTFs to thyroid dysgenesis and thyroid cancer are largely unknown (1). Therefore, the purpose of the present study was to examine the effects of re-expression of NKX2-1 on cell death in dedifferentiated thyroid cancer cells which lacked NKX2-1 expression. In addition, we analyzed the genes involved in NKX2-1-induced cell death to explore the mechanisms.

Materials and Methods

Cell culture

BHP18-21v and BHP7-13 cells, expressing *PAX8* but not *NKX2-1*, *FOXE1*, *TG,* or *TPO* genes (17), were kindly provided by Prof. J. M. Hershman (University of California, Los Angeles, CA, United States). These cells were derived from primary tumors with histological features of human papillary thyroid carcinoma (18), and were maintained in RPMI-1640 containing 10% fetal bovine serum (FBS) in 5% CO_2 at 37°C. DNA profiling of the BHP18-21v cell has already been shown in a previous report (19). MDCK (RIKEN RCB0995; Wako, Japan), a canine kidney epithelial cell line, expressing PAX8 but not NKX2-1, was cultured in Dulbecco's modified Eagle medium (DMEM), supplemented with 10% FBS. HepG2, a human hepatocellular cancer cell line, was purchased from American Type Culture Collection (Manassas, VA, United States) and cultured in DMEM containing 10% FBS. HepG2 cells express neither NKX2-1 nor PAX8.

Construction of recombinant adenoviral vectors

AdTTF-1 is a ΔE1-ΔE3 recombinant adenovirus expressing the rat *Nkx2-1* gene under the control of the immediate early promoter of cytomegalovirus (CMV). The NKX2-1 has 92.4% homology to the cDNA sequence, and > 98% to the amino acid sequence between human and rat. Construction of the AdTTF-1 virus has been previously described (17). AdLacZ, which contains the CMV promoter-controlled *lacZ* gene, was purchased from Quantum Biotechnologies (Montréal, Canada), and was used as a control. Recombinant adenoviruses were plaque-purified, harvested 72 hours (h) after infection of 293 cells, and purified using the ViraTrap™ Adenovirus Purification Maxi Kit (Biomiga, San Diego, CA, United States). Viral titers were determined by tissue culture

infectious dose 50 ($TCID_{50}$) using cultured 293 cells.

Quantification of cell viability

The BHP18-21v cells were seeded in 1.2×10^3 or 3.6×10^3 cells per well of a 96-well culture plate for the analyses of time- or multiplicity of infection (MOI)-dependencies, respectively. Adenoviral vectors were infected at the indicated MOI 24 h after plating BHP18-21v cells. Cell viability was quantified at the indicated time after infection using Cell Counting Kit-8 (CCK-8) (Dojindo, Mashiki, Japan) according to the manufacturer's protocol. After adding 10 μl CCK-8 solution to each well, incubation was continued for 90 minutes (min) before measuring absorbance using a microplate reader, Vairoskan LUX (Thermo Fisher Scientific, Waltham, MA, United States).

Detection of cellular apoptosis and necrosis

(1) Acridine orange and ethidium bromide staining

BHP18-21v cells cultured in 6-well plates were infected with 300 MOI of AdTTF-1 or AdLacZ. After incubation for 48 h, the cells were exposed to 2 μg/ml of acridine orange and 2 μg/ml of ethidium bromide in phosphate-buffered saline (PBS). The fluorescence was observed using a fluorescence microscope.

(2) Hoechst 33342 staining

BHP18-21v cells cultured on cover glasses were infected with 300 MOI of AdTTF-1 or AdLacZ. After incubation for 48 h, the cells were fixed with 1% glutaraldehyde, and then Hoechst 33342 staining was performed. The cells were then incubated in the presence of 2 mM Hoechst 33342 in the dark for 30 min at room temperature and then washed three times with PBS. The fluorescence

was observed using a fluorescence microscope.

(3) DNA isolation and DNA ladder detection by agarose gel electrophoresis

BHP18-21v cells were infected with 1000 MOI of AdTTF-1 or AdLacZ in 10-cm dishes. After incubation for 36 h, the cells were collected and homogenized. Their chromosomal DNA was extracted using DNeasy® Blood & Tissue Kit from QIAGEN (Hilden, Germany). DNA (0.25 μg) was labeled at room temperature for 30 min using 5 units of terminal deoxynucleotidyl transferase in a total of 50 μl containing 0.5 μCi of [α-^{32}P]dATP (6000 Ci/mmol; Amersham Pharmacia Biotech, Uppsala, Sweden) and separated on a 1.8% agarose gel with Tris-acetate EDTA buffer (40 mM Tris-acetate, 1 mM EDTA) as the running buffer. After they were dried on Whatman® 3 MM papers (Merck, Darmstadt, Germany), fragmented DNA bands were visualized using an image analyzer, BAS 2500 (Fujifilm, Tokyo, Japan).

(4) Realtime assay using annexine V

Annexine V and cell permeability were measured using the RealTime-Glo™ Annexin V Apoptosis and Necrosis Assay (Promega, Madison, WI, United States) in accordance with the manufacturer's recommendations. Briefly, BHP18-21v cells were seeded in triplicate into a 96-well plate (Nunc™ MicroWell™ Optical-Bottom Plates with Polymer Base; Thermo Fisher Scientific) with or without siRNA transfection and were cultured. The cells were infected with 300 MOI of AdTTF-1 or AdLacZ 24 h after seeding. After incubation for another 24 h, 500 × detection reagent, including Annexin V NanoBiT® substrate, $CaCl_2$, Necrosis detection reagent, Annexin V-SmBiT, and Annexin V-LgBiT, was added into each of the tested wells of the 96-well plate. Measurements of luminescence for apoptosis and fluorescence (485 nm_{Ex}/525 nm_{Em}) for necrosis

were performed at the indicated time after infection using a microplate reader, Varioskan LUX (Thermo Fisher Scientific).

Comprehensive analysis of the gene expressions

BHP18-21v cells incubated in 10-cm dishes were infected with 100 MOI of AdTTF-1 or AdLacZ. After incubation for 6, 12, and 24 h, the cells were collected. Total RNA was isolated from each of the frozen samples with RNeasy® Mini Kit (QIAGEN) for gene expression analysis. Gene expression profiles were determined using GeneChip™ Human Genome U113 plus 2.0 array (Affymetrix, Santa Clara, CA, United States) according to the manufacturer's recommendations. In brief, double-stranded cDNA was synthesized with 8 μg of total RNA with oligo d(T)24 T7 primer and transcribed into biotinylated cRNA using the IVT Labeling Kit (Affymetrix). Twenty μg of the biotinylated cRNA were fragmented at 94°C for 35 min and hybridized to the GeneChip array, which contains > 54,000 probe sets. The hybridized cRNA probes to oligonucleotide arrays were stained with streptavidin R-phycoerythrin and scanned using GeneChip™ Scanner 3000 (Affymetrix). The scanned data were processed for signal values using Microarray Suite 5.0 software (Affymetrix). All data used for the subsequent analysis passed the quality control criteria according to the manufacture’s protocol.

Determination of mRNA levels

Total RNA was isolated from cultured cells using an RNeasy® Mini Kit. After quantification by spectrophotometry, 5 μg total RNA was reverse-transcribed into cDNA using SuperScript® III First-Strand Synthesis System for RT-PCR (Thermo Fisher Scientific). Oligonucleotide primers, including TaqMan Probes for arginase 2 (ARG2) (Hs00982833_m1), regulator of G protein

signaling 4 (RGS4) (Hs01111690_g1), and RGS5 (Hs01591223_s1), were purchased from Thermo Fisher Scientific. To normalize differences in the amount of cDNA added to the reactions, amplification of 18S or glyceraldehyde-3-phosphate dehydrogenase (GAPDH) was performed as an endogenous control. Primers and probes for 18S (Hs99999901_s1) and GAPDH (Hs99999905_m1) were purchased from Thermo Fisher Scientific. Real-time PCR was achieved in 96 sample tubes using the cDNA equivalent to 100 ng of RNA with 1 × TaqMan® Universal Master Mix II with Uracil-N-Glycosylase (UNG) (Thermo Fisher Scientific), 900 nM of each primer, and 400 nM TaqMan probe. The cycling conditions included an initial phase of 2 min at 50°C, followed by 10 min at 95°C required for optimal UNG enzyme activity, 50 cycles of 15 seconds at 95°C, and 1 min at 60°C. Polymerization reactions were performed in a StepOnePlus™ Real-Time PCR System (Thermo Fisher Scientific).

Gene expression data were analyzed using the comparative C_T method ($\Delta\Delta C_T$) (20). 18S or GAPDH was used as the reference gene. Missing values occurred where gene expression was below the limit of detection after 45 cycles of PCR.

siRNA transfection to target ARG2, RGS4, and RGS5

Three predesigned validated siRNAs for human *ARG2* (*Silencer*® Select; s1571, s1572, and s1573 [siARG2#1, siARG2#2, and siARG2#3, respectively]), and three predesigned siRNAs for human *RGS4* (*Silencer*® Select; s11992, s230181, and s230182 [siRGS4#1, siRGS4#2, and siRGS4#3, respectively]), and human *RGS5* (*Silencer*® Select; s16121, s16122, and s224973 [siRGS5#1, siRGS5#2, and siRGS5#3, respectively]) were purchased from Thermo Fisher Scientific, because there are a considerable variations in silencing efficiency among siRNAs.

Five nM of each siRNA was individually transfected into BHP18-21v cells with

Lipofectamine™ RNAiMAX Transfection Reagent (Thermo Fisher Scientific). siRNA transfection was performed according to the manufacturer's protocol for the "reverse transfections". First, each siRNA was diluted in Opti-MEM® Medium (Thermo Fisher Scientific). Lipofectamine™ RNAiMAX was then added to the diluted siRNA. After incubation of the complexes for 15 min at room temperature, cells diluted in growth medium were added. At 24 h after the siRNA transfection, the cells were infected with adenoviral vectors, then incubated further for indicated times, and assays were performed. To monitor siRNA delivery efficiency, we measured *GAPDH* (*Silencer*® Select GAPDH Positive Control; Thermo Fisher Scientific) mRNA levels by real-time PCR. Nonspecific siRNA (*Silencer*® Select Negative Control No.1 [siNegative]; Thermo Fisher Scientific) was used as a negative control.

Statistical analysis

Statistical analyses were carried out using the statistical software IBM SPSS Statistics 26 (IBM, Armonk, NY, United States). All data are expressed as the mean ± standard error of the mean (SEM). Differences between the groups were examined for statistical significance using Student's *t* test, and a p value of < 0.05 was considered significant.

Results

AdTTF-1-induced cell death in BHP18-21v cells

Time-dependent changes in the viability of the BHP18-21v cells after infection with adenoviral vectors were investigated using CCK-8. Cell viability was measured after 24, 72, 120, and 168 h of incubation with 1000 MOI of AdTTF-1 or AdLacZ. The percentages of the ratios of survived infected cells to survived non-infected cells at the same measuring time are shown in **Figure 1A**. The differences in these percentages between AdTTF-1-infected cells and AdLacZ-infected cells were statistically analyzed. The percentages of survival 72, 120 and 168 h after infection were significantly decreased in AdTTF-1-infected cells compared to those in AdLacZ-infected cells.

MOI-dependent changes of cell death induced by infection with AdTTF-1 or AdLacZ were also analyzed (**Figure 1B**). After 120 h of incubation with 1, 3, 10, 30, 100, 300, 1000, 3000, or 10000 MOI of adenoviral vectors, cell viability was measured. The percentages of survival of the BHP18-21v cells infected with 300, 1000, and 3000 MOI of AdTTF-1 were significantly decreased compared to those of the AdLacZ-infected cells.

For the purpose of investigating whether AdTTF-1 causes cell death in another cell line derived from papillary thyroid carcinoma, BHP7-13 cells ($NKX2\text{-}1^{-}/PAX8^{+}$) were infected with AdTTF-1 or AdLacZ. The percentages of survival of the BHP7-13 cells infected with 30, 100, 300, 1000, and 3000 MOI of AdTTF-1 were also significantly decreased compared to those of the AdLacZ-infected cells. To examine the non-thyroid cells, MDCK cells ($NKX2\text{-}1^{-}/PAX8^{+}$) and HepG2 cells ($NKX2\text{-}1^{-}/PAX8^{-}$) were infected with AdTTF-1 or AdLacZ. In contrast to the BHP18-21v and BHP7-13 cells, there were no significant differences between the AdTTF-1-infected cells and the AdLacZ-infected cells, except MDCK cells infected at 30 and 10000 MOI and HepG2 cells

infected at 3000 MOI. These results suggest that infection with AdTTF-1 induced cell death only in thyroid cancer cells.

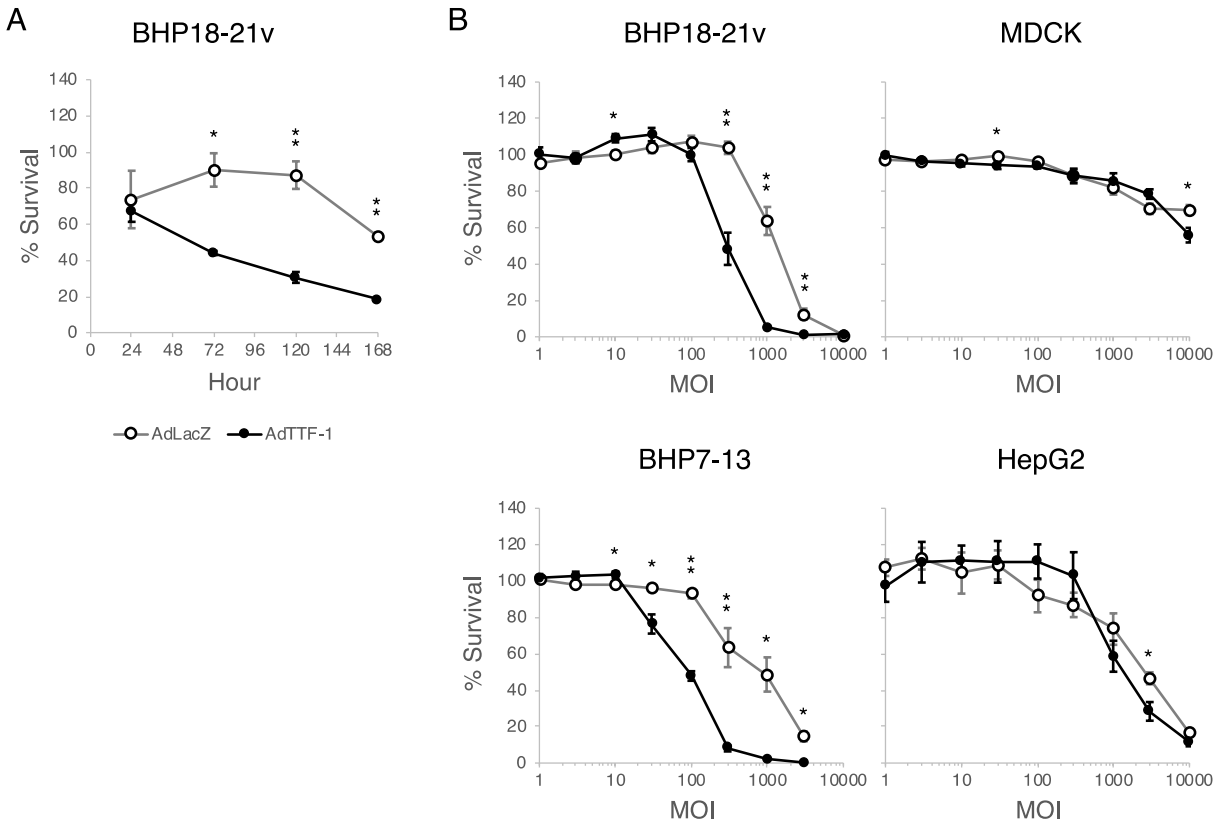

Figure 1. Cell viability after infection with AdTTF-1

A: Time-dependent changes after infection with 1000 MOI of adenoviral vectors.

B: MOI-dependent changes 120 h after infection with adenoviral vectors.

The ratios of survived infected cells to survived non-infected cells at the same measuring time are shown. Closed and open circles represent AdTTF-1- and AdLacZ-infected cells, respectively. Error bars represent SEM. Asterisks show significant differences between AdTTF-1 and AdLacZ (*, P <0.05; **, P <0.01). MOI, multiplicity of infection

AdTTF-1-induced apoptosis and necrosis in BHP18-21v cells

In order to analyze the mechanisms of BHP18-21v cell death induced by infection with AdTTF-1, acridine orange and ethidium bromide double stain and Hoechst 33342 stain were performed 48 h after infection with 300 MOI of adenoviral vectors to detect the apoptotic and necrotic cells. The acridine orange and ethidium bromide double stain showed only a few necrotic cells among the AdLacZ-infected cells; however, both necrotic cells and apoptotic cells in the early or late phase were clearly observed among the AdTTF-1-infected cells (**Figure 2A**). The Hoechst 33342 stain revealed apoptotic cells with a condensed nucleus and necrotic cells with a ballooning nucleus in the AdTTF-1-infected cells, but not in the AdLacZ-infected cells (**Figure 2B**). Induction of both apoptosis and necrosis in the AdTTF-1-infected BHP18-21v cells was also examined by detection of DNA fragmentation. DNA was isolated 36 h after infection with adenoviral vectors. Both ladder and smear patterns of the DNA fragmentation, which represented apoptosis and necrosis, respectively, were observed in the AdTTF-1-infected cells. In contrast, no band was detected in the AdLacZ-infected cells (**Figure 2C**). Real-time assays for detection of apoptosis and necrosis were also performed to analyze time-dependent changes after infection with 300 MOI of adenoviral vectors. The signals of luminescence (apoptosis signal) and fluorescence (necrosis signal) in the controls (non-infected BHP18-21v cells), AdTTF-1-infected cells, and AdLacZ-infected cells are shown in **Figure 2D**. The apoptosis signals in the AdTTF-1-infected cells were significantly increased compared to those in the AdLacZ-infected cells between 48 and 128 h after infection. On the other hand, the necrosis signals in the AdTTF-1-infected cells were significantly increased from 56 h after the infection compared to those in the AdLacZ-infected cells. Taken together, it was demonstrated that the infection with AdTTF-1 induced both apoptosis and necrosis in BHP18-21v cells.

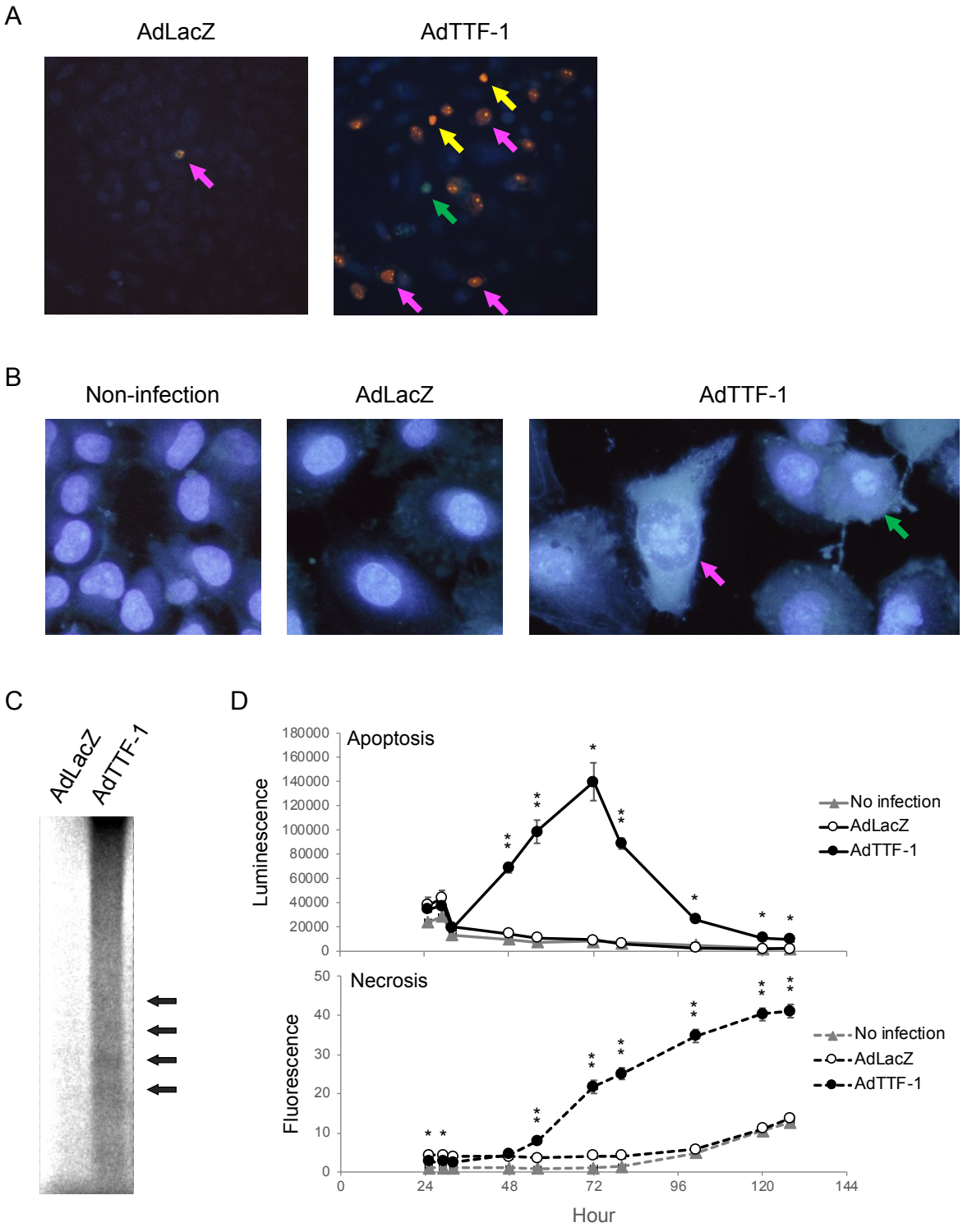
A
AdLacZ
AdTTF-1
B
Non-infection
AdLacZ
AdTTF-1
C
AdLacZ
AdTTF-1
D
Apoptosis
Luminescence
180000
160000
140000
120000
100000
80000
60000
40000
20000
0
No infection
AdLacZ
AdTTF-1
Necrosis
Fluorescence
50
40
30
20
10
0
0
24
48
72
96
120
144
Hour

Figure 2. Detection of apoptosis and necrosis after infection with AdTTF-1
A: Acridine orange- and ethidium bromide-stained BHP18-21v cells. The green, yellow and magenta arrows represent early apoptotic cells (condensed chromatin stained by acridine orange), late apoptotic cells (condensed chromatin stained by ethidium bromide) and necrotic cells (normal chromatin stained by ethidium bromide), respectively.
B: Hoechst 33342-stained BHP18-21v cells. The green and magenta arrows represent apoptotic and necrotic cells, respectively.
C: Agarose gel electrophoresis of isolated DNA from BHP18-21v cells. Arrows show the ladder bands which represent DNA fragmentation caused by apoptosis.
D: Real-time assay. Closed and open circles represent the AdTTF-1- and AdLacZ-infected cells, respectively. Gray triangles represent non-infected cells. Error bars represent SEM. Asterisks show significant differences between AdTTF-1 and AdLacZ (*, P <0.05; **, P <0.01). MOI, multiplicity of infection

GeneChip analysis after AdTTF-1 infection

To explore the mechanism of BHP18-21v cell death induced by infection with AdTTF-1, the gene expressions after infection with adenoviral vectors were analyzed comprehensively using GeneChip microarrays. The gene expressions in the AdTTF-1-infected cells were compared to those in the AdLacZ-infected cells at 6, 12, and 24 h after infection. The analyses were performed on 54613 transcripts. The ratio of gene expression in the AdTTF-1-infected cells to that in the AdLacZ-infected cells was twice or higher in 199, 314, and 1482 genes at 6, 12, and 24 h, respectively (**Figure 3A**). On the other hand, that ratio was 0.5-fold or less in 15, 62, and 838 genes at 6, 12, and 24 h, respectively (**Figure 3B**). The analysis based on the Gene Ontology resource showed that infection with AdTTF-1 induced significant increases in expression of genes that were categorized into the following categories: Regulation of signal transduction, Regulation of G-protein coupled receptor protein signaling pathway, Negative regulation of cellular process,

Negative regelation of biological process, Telomerase-dependent telomere maintenance, Lysine catabolism, and Positive regulation of cell proliferation. **Table 1** shows a list of individual genes whose expression was largely increased by infection with AdTTF-1. The signal intensities of gene expressions in the AdTTF-1- and AdLacZ-infected cells and the ratios of the intensities (AdTTF-1/AdLacZ) at each measuring time are also shown in **Table 1.**

For further investigation, we selected three genes, *ARG2*, *RGS4*, and *RGS5*, from the list in Table 1 based on the following criteria: there was an apparent expression at 6 h after infection; the ratio at 12 h was more than twice; and the ratio at 24 h was more than ten-fold. The genes whose expressions did not increase at 6 h were excluded, as we considered that the genes whose expressions increased immediately after infection with AdTTF-1 were the direct target genes for NKX2-1. Although the ratios in the 28 kDa A-kinase anchoring protein (*AKAP28*) gene remarkably increased, the gene was excluded, since the signals in the AdTTF-1-infected cells did not increase at all. The matrix metallopeptidase 1 (*MMP1*) and mitogen-activated protein kinase kinase 5 (*MAP2K5*) genes were also excluded, since their expressions evaluated by real-time PCR did not result in an increase in AdTTF-1-infected BHP18-21v cells. In addition, the Nik related kinase (*NRK*) gene was excluded because its signal intensity was statistically unreproducible in the GeneChip microarrays.

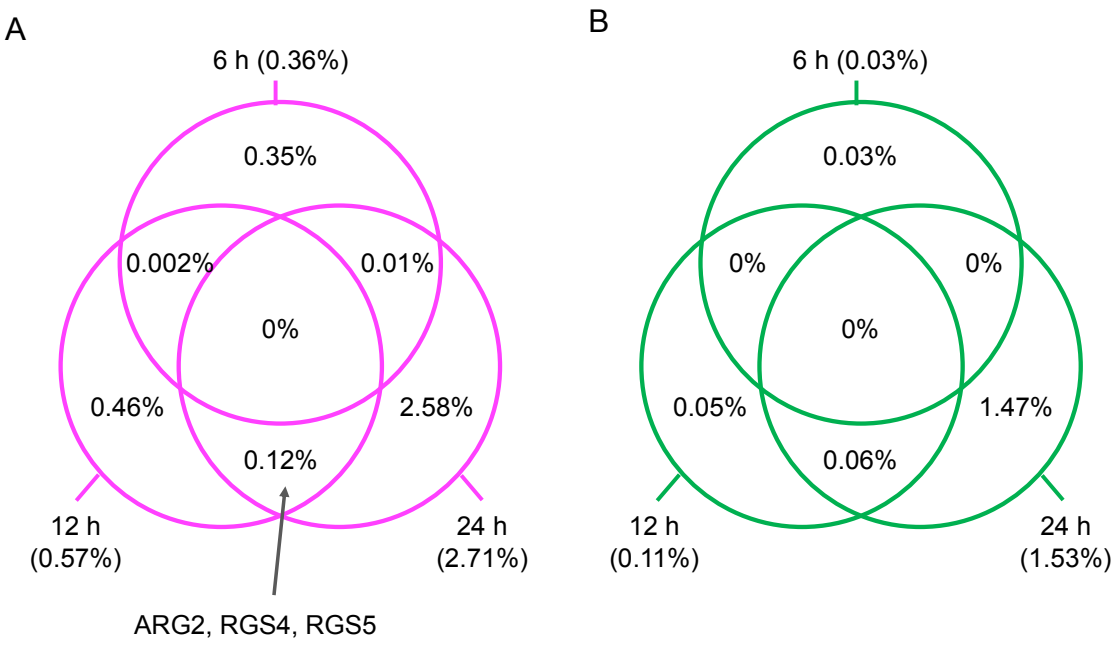

Figure 3. The percentages of genes whose expressions were largely different between in the AdTTF-1-infected cells and the AdLacZ-infected cells in GeneChip analyses at 6, 12, and 24 h after infection. A total of 54613 transcripts were analyzed.

A: The percentages of genes whose ratio of gene expression in the AdTTF-1-infected cells to that in the AdLacZ-infected cells was twice or higher. B: The percentages of genes whose ratio of gene expression in the AdTTF-1-infected cells to that in the AdLacZ-infected cells was 0.5-fold or lower.

Table 1. GeneChip analyses after AdTTF-1 infection

Genes (Probe set)	Gene expression								
	AdTTF-1			AdLacZ			Ratio (AdTTF-1/AdLacZ)		
	6 h	12 h	24 h	6 h	12 h	24 h	6 h	12 h	24 h
AKAP28	0.76	1.02	1.65	1.24	0.75	(0.03)	0.61	1.36	47.88
RGS5 (1555725_a_at)	(1.23)	2.65	30.98	(0.77)	(1.15)	0.69	1.58	2.30	45.07
RGS5 (218353_at)	1.24	2.04	21.14	0.76	(0.32)	0.60	1.64	6.46	35.46
RGS5 (209071_s_at)	1.06	3.65	46.39	0.94	0.88	1.32	1.13	4.14	35.26
ARG2	1.12	0.95	17.51	0.88	0.47	0.65	1.27	2.00	26.88
MMP1	0.93	1.74	22.57	1.07	0.91	1.11	0.88	1.91	20.27
FLJ10156	1.08	0.76	2.43	0.92	(0.64)	(0.14)	1.18	1.20	16.80
RRAGC	(0.69)	1.41	1.43	1.31	0.93	(0.09)	0.53	1.51	15.43
MAP2K5	1.58	3.54	5.09	(0.42)	(0.23)	(0.37)	3.73	15.70	13.74
cDNA clone IMAGE:4816369	(0.71)	1.57	2.32	(1.29)	1.41	(0.19)	0.55	1.11	12.11
RGS4 (204337_at)	1.04	2.36	4.74	0.96	0.61	0.43	1.08	3.89	11.16
KRTAP7-1	0.86	1.72	(1.33)	(1.14)	1.16	(0.12)	0.75	1.48	10.86
cDNA clone IMAGE:2737354	(0.95)	1.95	2.41	(1.05)	1.49	(0.22)	0.90	1.31	10.75
NRK	(1.02)	2.31	10.58	(0.98)	0.35	1.00	1.05	6.58	10.59

The list of genes whose expression was largely increased by infection with AdTTF-1. The signal intensities of gene expressions in the AdTTF-1- and AdLacZ-infected cells and the ratios of the intensities (AdTTF-1/AdLacZ) at each measuring time are shown. Genes are listed in descending order of ratio at 24 h after infection. Numbers in parentheses show signal intensities regarded as insignificant in the statistical investigations using GeneChip microarrays.

AKAP28, 28 kDa A-kinase anchoring protein; RGS, regulator of G protein signaling; ARG2, arginase 2; MMP1, matrix metallopeptidase 1; FLJ, full-length long Japan; RRAGC, Ras related GTP binding C; MAP2K5, mitogen-activated protein kinase kinase 5; KRTAP7-1, keratin associated protein 7-1; NRK, Nik related kinase

AdTTF-1-enhanced expression of ARG2, RGS4, and RGS5 in BHP18-21v cells

Quantification of mRNA levels by real-time PCR 72 h after infection was performed. The ratios of expression levels of *ARG2*, *RGS4*, and *RGS5* genes in the AdTTF-1- or AdLacZ-infected cells to those of the non-infected cells at 72 h are shown in **Figure 4A**. MOI-dependent increases in *ARG2*, *RGS4*, and *RGS5* mRNA levels were observed in the AdTTF-1-infected BHP18-21v cells. The expression levels of *ARG2* and *RGS4* in the AdTTF-1-infected cells at 30, 100, and 300 MOI were significantly higher than those in the AdLacZ-infected cells. The expression levels of *RGS5* in the AdTTF-1-infected cells at 30 and 100 MOI were significantly higher than those in the AdLacZ-infected cells.

To examine the time course, quantification of mRNA levels was also performed 6, 12, 24, 48, 72, and 96 h after infection with 300 MOI of adenoviral vectors. The ratios of expression levels of *ARG2*, *RGS4*, and *RGS5* genes in the AdTTF-1- or AdLacZ-infected cells to those of the pre-infected cells at 0 h are shown in **Figure 4B**. The time-dependent increases in the expression levels of the *ARG2*, *RGS4*, and *RGS5* genes were seen up to 72 h in the AdTTF-1-infected cells. However, the AdLacZ-infected cells exhibited no increase in these gene expressions.

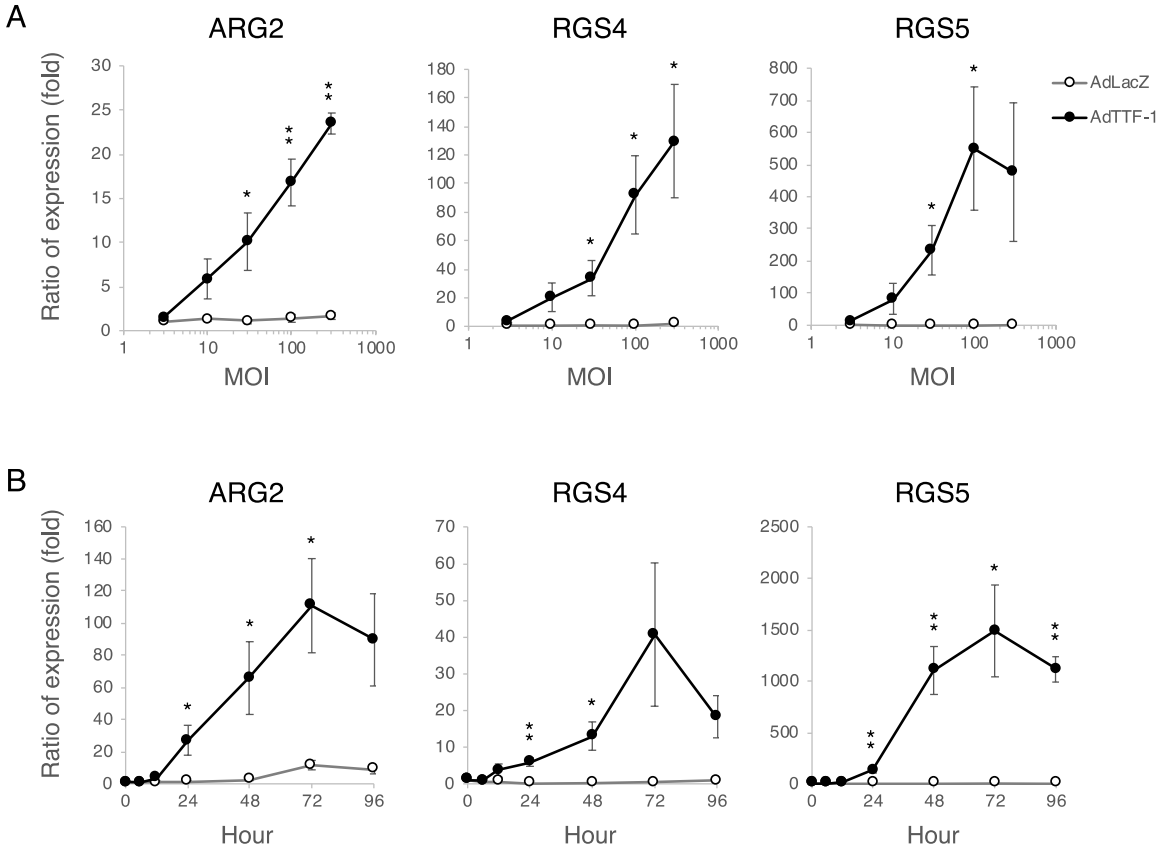

Figure 4. Gene expression after infection with AdTTF-1

A: MOI-dependent changes 72 h after infection with adenoviral vectors.

B: Time-dependent changes after infection with 300 MOI of adenoviral vectors.

Ratios of gene expressions in infected cells to those in non-infected cells at 72 h (A) or pre-infected cells (0 h) (B) are shown. Closed and open circles represent the AdTTF-1- and AdLacZ-infected cells, respectively. Error bars represent SEM. Asterisks show significant differences between AdTTF-1 and AdLacZ (*, P <0.05; **, P <0.01). MOI, multiplicity of infection

Effects of siARG2, siRGS4, and siRGS5 transfection in AdTTF-1-infected BHP18-21v cells

To demonstrate the efficiency of siRNA-mediated gene silencing, the BHP18-21v cells were transfected with siRNAs targeting three different mRNA regions in each of the genes;

siARG2#1−#3, siRGS4#1−#3, and siRGS5#1−#3. Nonspecific siRNA was used as negative control (siNegative). The quantification of mRNA expression was performed using real-time PCR after infection with 100 MOI of AdTTF-1. All the siRNAs targeting *ARG2*, *RGS4*, and *RGS5* efficiently down-regulated each of the mRNA expressions in the AdTTF-1-infected BHP18-21v cells (**Figure 5**). The percentages of the ratios of mRNA expression in the cells transfected with siARG2, siRGS4, or siRGS5 to that in the cells transfected with siNegative ranged from 2.9 ± 0.7% to 12.7 ± 0.5%. The most efficient silencing was obtained with siARG2#2, siRGS4#2, and siRGS5#3, which were used for further experiments using siRNA transfection.

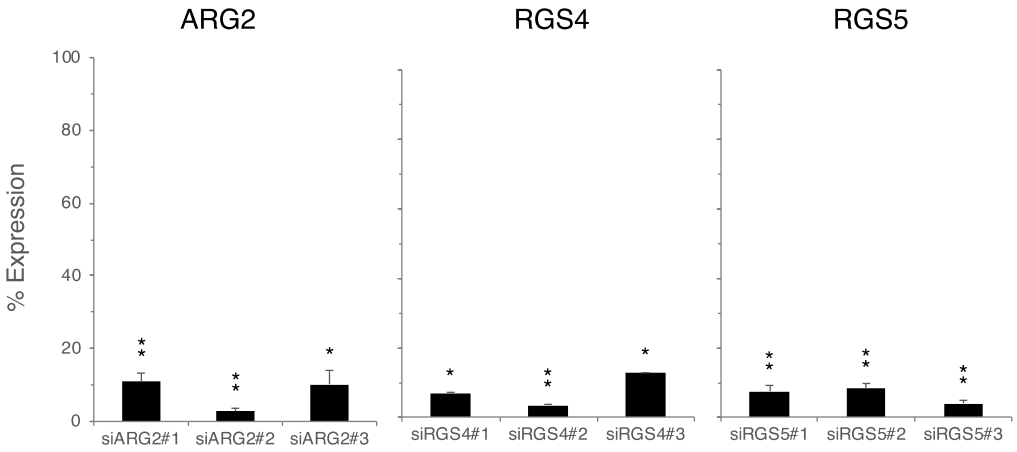

Figure 5. Gene expression in siRNA-transfected cells after infection with AdTTF-1
mRNA expression in siARG2-, siRGS4-, or siRGS5-transfected cells are shown in percent of control. siNegative-transfected cells were used for the control. Error bars represent SEM. Asterisks show significant differences between siNegative and siRNA for *ARG2*, *RGS4*, or *RGS5* (*, $P < 0.05$; **, $P < 0.01$).

For the purpose of investigating the effects of the *ARG2*, *RGS4*, and *RGS5* genes on cell death caused by AdTTF-1-infection, cell viability was measured in siRNA-transfected BHP18-21v cells 72 h after infection with 300 MOI of AdTTF-1. The percentages of the ratios of survived cells in the siARG2#2-, siRGS4#2-, and siRGS5#3-transfected cells to those in the negative control (siNegative-transfected cells) are shown in **Figure 6A**. Cell viabilities in the siARG2#2-, and siRGS4#2-transfected cells were significantly higher (115.7 ± 2.7% and 113.2 ± 4.2%, respectively) than those in the negative control. These results indicate that suppression of *ARG2* or *RGS4* gene expression significantly, but partially, inhibited cell death induced by AdTTF-1 infection. On the other hand, there was no significant difference in cell viability between the siRGS5#3-transfected cells and the negative control cells.

To examine the effects of the *ARG2*, *RGS4*, and *RGS5* genes on apoptosis and necrosis caused by AdTTF-1-infection, real-time assays for detection of apoptosis and necrosis were performed in BHP18-21v cells transfected with siARG2#2, siRGS4#2, and siRGS#3. Apoptosis signals and necrosis signals were analyzed at 72 and 96 h, respectively, after infection with 300 MOI of AdTTF-1. These measuring times were selected based on the results of the preceding real-time assays without the siRNA transfection mentioned above (**Figure 2D**). The percentages of the ratios of intensity of luminescence (apoptosis) or fluorescence (necrosis) in the cells transfected with siARG2#2, siRGS4#2, or siRGS5#3 to those in the negative control are shown in **Figure 6B**. The luminescence in the siARG2#2- and siRGS4#2-transfected cells were significantly decreased to 82.4 ± 3.7% and 71.5 ± 5.4%, respectively. The fluorescence in these cells were also decreased to 78.7 ± 6.1% and 62.3 ± 8.6%, respectively. On the other hand, in the siRGS5#3-transfected cells, the luminescence was significantly increased (126.9 ± 8.9%), and the fluorescence did not significantly differ from that in the negative control cells. These results indicate that suppression

of *ARG2* or *RGS4* gene expression significantly, but partially, inhibits apoptosis and necrosis induced by AdTTF-1 infection.

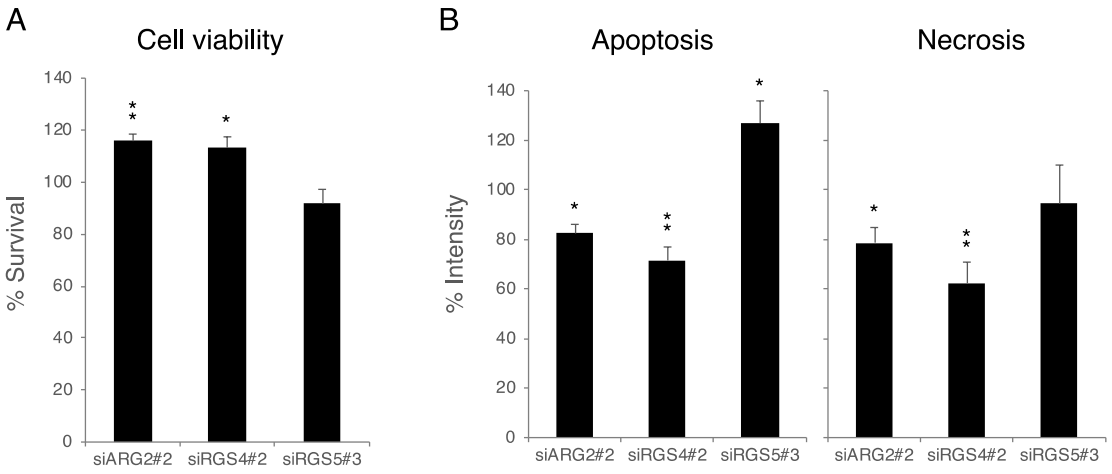

Figure 6. The effects of siRNAs on AdTTF-1-induced cell death, apoptosis, and necrosis

A: Cell viability of siRNA-transfected cells after infection with AdTTF-1. Amounts of survived cells in siARG2-, siRGS4-, or siRGS5-transfected cells are shown in percent of control.

B: Apoptosis and necrosis in siRNA-transfected cells after infection with AdTTF-1. Intensities of apoptosis and necrosis signal in siARG2-, siRGS4-, or siRGS5-transfected cells are shown in percent of control.

siNegative-transfected cells were used for the control. Error bars represent SEM. Asterisks show significant differences between siNegative and siRNA for *ARG2*, *RGS4*, or *RGS5* (*, $P < 0.05$; **, $P < 0.01$).

Discussion

In general, thyroid cancer is a disease with a good prognosis. However, poorly differentiated thyroid carcinoma (PDTC), whose reported incidence ranges from 2% to 15% of all thyroid cancers, induced distant metastases in up to 85% of cases (21). Moreover, the one-year disease-specific survival rate was shown to be 34.3% in anaplastic thyroid carcinoma, which is one of the most virulent and aggressive of all malignancies (22), because of the rapid invasion of adjacent structures and the metastasis throughout the body. In dedifferentiated thyroid carcinoma cells, the levels of NKX2-1 expression were decreased (12). In the present study, it was demonstrated that cell death was induced by transduction of the *NKX2-1* gene using the adenoviral vector into dedifferentiated thyroid carcinoma cells that do not express NKX2-1. In addition, we also showed that re-expression of NKX2-1 caused cell apoptosis and necrosis in those cells.

In the present study, cell death was observed in BHP18-21v and BHP7-13 cells after infection with AdTTF-1. As these thyroid cancer cells expressed PAX8 but not NKX2-1, the cell death was seemingly due to effects induced by the re-expression of NKX2-1. However, the analyses of cell viabilities in non-thyroid cells showed that AdTTF-1-infection did not cause cell death in HepG2 liver cells, which expressed neither the PAX8 nor the NKX2-1. In addition, cell death was not induced in MDCK kidney cells expressing PAX8 but not NKX2-1, whose expression pattern was identical to the thyroid cancer cells used in this study. Thus, cell death did not occur in non-thyroid cells in spite of the expression of PAX8. These findings indicated that AdTTF-1-induced cell death was an exclusive effect on thyroid cancer cells. We previously reported that AdTTF-1-infection in thyroid cancer cells not expressing NKX2-1 induced activation of the TG promoter. However, MDCK cells exhibited only faint activation of the TG promoter (17). Although both NKX2-1 and

PAX8 had key roles in activating the TG promoter, co-expression of these two genes did not induce activation of this promoter in non-thyroid cells. The results in our previous study implied that the difference in TG promoter activation among tissues was related to epigenomic distinction. Similar mechanisms may account for the induction of cell death only in thyroid cancer cells in the present study.

There are three distinct cell death morphologies; apoptosis, necrosis, and cell death associated with autophagy (23). On apoptosis and necrosis assays using four different methods, it was demonstrated that the infection with AdTTF-1 caused both apoptosis and necrosis in BHP18-21v cells. Griesing *et al.* reported that NKX2-1-regulated microRNA induced apoptosis in lung adenocarcinoma cells (24). In addition, the fact that *NKX2-1* gene transduction increased cellular apoptosis in non-small cell lung cancer suggests that NKX2-1 might serve as a tumor suppressor gene (25). With regard to necrosis, the term necroptosis is defined as regulated necrosis that is dependent on receptor-interacting protein kinase (RIPK) 1 and/or RIPK3 activity (26). Vanden Berghe *et al.* have described regulated necrosis as a genetically controlled cell death process that eventually results in cellular leakage (23). Necroptosis is triggered by death ligands such as tumor necrosis factor (TNF), Fas ligand (FasL), and TNF-related apoptosis inducing ligand (TRAIL), especially under the condition when apoptosis is inhibited. Nehs *et al.* previously reported necroptosis related to radiation-induced cell death in anaplastic thyroid cancer (27). In the present study, necrosis was detected in the process of programmed cell death caused by AdTTF-1. Therefore, we considered that the necrosis in our study might be necroptosis. Necroptosis was reported to be incompatible with apoptosis because it was identified as a backup and alternative to apoptosis (23). However, Lin *et al.* have recently reported the simultaneous induction of apoptosis and necroptosis caused by a herbal medicine in HepG2 cells (28).

NKX2-1 is one of the homeobox genes encoding a family of homeodomain-containing transcription factors that play important roles in the early embryo, including the establishment of cell and tissue identity, and the regulation of cell proliferation, differentiation, and survival (29). Concerning cancers, the various functions of homeobox genes, such as prospero homeobox 1 (*PROX1)* (30), zinc finger E-box binding homeobox 1 (*ZEB1*) (31), and NK-like (NKL) homeobox gene (32), have been reported. Homeodomain-containing proteins are able to both activate and repress transcription of genes in a context-dependent manner (30). In the present study, the comprehensive gene analysis using GeneChip microarrays after AdTTF-1-infection identified the genes whose expressions were greatly increased. These genes belong to groups particularly related to regulation of signal transduction, regulation of G-protein coupled receptor protein signaling pathway, negative regulation of cellular and biological processes, telomerase-dependent telomere maintenance, lysine catabolism, and positive regulation of cell proliferation. These results indicated that homeobox gene expression diversely regulates the expression levels of a wide variety of genes.

Regarding the individual gene that were increased by AdTTF-1, we focused on three: *ARG2*, *RGS4*, and *RGS5*. Arginase catalyzes the conversion of arginine to ornithine and urea, indicating that the increase of arginase expression induces the reduction of arginine. While ARG1 is located in the cytosol and is mainly expressed in the liver, ARG2 is located in the mitochondrial matrix and is expressed in extra-hepatic tissues (33). Arginine has a pivotal role in cellular physiology as it is involved in numerous cellular metabolic and signaling pathways. Thus, arginine deprivation therapy (ADT) has been proposed as a potential anti-cancer therapy (34). On the other hand, arginine is also a common substrate for nitric oxide (NO) synthase. The depletion of arginine suppresses NO synthesis, which is also another possible mechanism for ADT. Accordingly, we

considered that the increase in ARG2 induced by NKX2-1 might affect cell death via arginine deprivation including inhibition of NO generation. There have been several reports concerning the relationship between ARG2 expression and cancer in a variety of organs, including the thyroid. Sousa *et al*. reported that ARG2 expression was increased in differentiated thyroid carcinoma but not in benign lesions or normal tissues, and they suggested that ARG2 worked in coordination with endothelial NO synthase for tumorigenesis and/or tumor progression (35). Singh *et al*. investigated the expression and biological activity of arginase, mainly due to ARG2 rather than ARG1, in different human breast cancer cell lines, and reported that some cell lines had high arginase activity, while others had very low activity (36). Mumenthaler *et al*. demonstrated that ARG2 was differentially expressed depending on the stage of tumor development in a mouse model of transgenic prostate adenocarcinoma. In this model, ARG2 expression was not detected in advanced prostate tumors (37). These studies imply that the association of ARG2 expression and tumor proliferation would be much dependent on the cell characteristics, tissue types, and stages of cancer progression.

RGS proteins modulate the physiological actions of many neurotransmitters, hormones, and other signaling molecules. Human RGS proteins comprise a family of 20 canonical proteins that bind directly to G protein-coupled receptors or G protein complexes to limit the lifetime of their signaling events, which regulate all aspects of cell and organ physiology (38). All canonical RGS proteins share a conserved, approximately 120 amino acid RGS domain. While RGS4 is selectively expressed in the heart and brain, RGS5 is found broadly in tissues (38). The function of RGS4 was to respond to cardiovascular stress and modulate neuronal signaling. The relations of *RGS4* mRNA and neurological diseases, such as schizophrenia (39), Alzheimer's disease (40), and alcoholism (41), have been reported. There also have been reports showing that RGS4 expressions suppressed

breast cancer migration, invasion, and proliferation (42) (43), and that the *RGS4* gene reduced risk of bladder cancer with the increasing number of variant alleles (44). On the other hand, RGS5 plays a role in controlling vascular remodeling (38). It was reported that RGS5 was downregulated in atherosclerotic plaques (45), and was responsible for the abnormal tumor vascular morphology (46). As mentioned above, although several reports showed the associations between ARG2, RGS4, or RGS5 and cancers, no reports described the effects of *NKX2-1* gene on any of these three genes.

Furthermore, to investigate the effect of the *ARG2*, *RGS4*, and *RGS5* genes on cell death caused by AdTTF-1-infection in the present study, we analyzed cell viability, apoptosis and necrosis in siRNA-transfected cells. The suppression of each *ARG2* and *RGS4* gene expression reduced cell death after the re-expression of NKX2-1. In addition, the inhibition of ARG2 or RGS4 expression also repressed apoptosis and necrosis. These results indicated that ARG2 and RGS4 have a partial role in suppressing survival of dedifferentiated thyroid cancer cells. The involvement of apoptosis or non-apoptotic cell death in cell death mechanisms in arginase-mediated ADT (47) (48) (49) or arginase inhibition (35) (36) (50) has been reported. Whether the overexpression of arginase inhibits or induces cancer progression might depend on the context condition; the cell characteristics, tissue types, and stages of cancer progression. Similarly, there have been conflicting reports on the role of RGS4 in cancer. Xue *et al*. found that endogenous RGS4 expression was lower in melanoma cells (51). They reported that RGS4 could reduce the proliferation, migration, and invasion of melanoma cells, and the apoptosis rate was significantly decreased in the low RGS4 environment. Furthermore, Xiao *et al.* reported that overexpression of microRNA-107 in hepatocellular carcinoma cells suppressed cellular proliferation, invasion, migration and colony-forming ability, but promoted apoptosis and G1 phase arrest by modulating RGS4 expression (52). These previous reports showed that RGS4 overexpression induced apoptosis in cancer cells. In

contrast, He *et al*. reported an increase in RGS4 protein level in non-small cell lung cancer cells (53). They demonstrated that RGS4 knockdown inhibited cell proliferation and induced apoptosis, and that RGS4 negatively regulated microRNA-16, a tumor suppressor. In the case of thyroid cancer, it has been reported that overexpression of *RGS4* gene induced an inhibition of microRNA-3663-3p expression and an increase in expression of RPL34-AS1, a long non-coding RNA, which resulted in the induction of apoptosis as well as the inhibition of proliferation and invasion in papillary thyroid cancer cells (54). Based on these reports, we consider that the function of RGS4 varies among types of cancers.

Concerning the RGS5, Altman *et al.* reported that RGS5 expression reduced ovarian cancer cells, and that mice bearing RGS5-expressing tumors demonstrated an increase in survival compared with controls (55). They suggested that those tumor-suppressive effects were independent of the role of RGS5 in vascular normalization and remodeling. Xu *et al.* also showed that RGS5 played an inhibitory role in human lung cancer cells (56). They reported that RGS5 overexpression induced apoptosis in the lung cancer cells, and lower adhesion and migration abilities of those cells. In the present study, the suppression of RGS5 by siRNA did not significantly affect the cell death induced by the NKX2-1. In addition, apoptosis was increased when the RGS5 expression was inhibited. These results were inconsistent with the previous reports on the RGS5, and suggested that the effects of RGS5 on cell viability might be cancer-specific.

We demonstrated that the expression of homeobox *NKX2-1* gene using adenoviral vectors led to cell death in *NKX2-1*-non-expressing thyroid carcinoma cell lines. Abate-Shen reported in a review that both losses and gains of homeobox gene expression are associated with tumorigenesis (57). The author described that most reported cases of deregulated homeobox gene expression in cancer conformed to a rule in which the homeobox genes that are normally expressed in undifferentiated

cells are upregulated in cancer, whereas those that are normally expressed in differentiated tissues are downregulated in cancer. Regarding lung cancer, *NKX2-1* has pro- and anti-oncogenic activities (58). Yamaguchi *et al.* showed that *NKX2-1* played a role as a lineage-survival oncogene as well as a suppressor of cancer progression in lung adenocarcinomas (16). For the reason for NKX2-1 functioning as a double-edged sword in the pathogenesis of lung adenocarcinoma, they suggested that NKX2-1 is transcribed under the influence of various transcription factors, and its transcriptional regulatory activities are modulated in a context-dependent manner by cooperating transcription factors as well as protein modifications. Li *et al.* reported that the developmental transcription factors forkhead box A2 (FOXA2) and caudal type homeobox 2 (CDX2) function cooperatively with NKX2-1 as important regulators in inhibiting metastasis of lung adenocarcinoma (59). They described these three transcription factors to be consistently down-regulated in metastatic cells compared with nonmetastatic cells. Tomida *et al.* reported that enforced expression of the distal-less homeobox 4 (*DLX4*) gene, which was reduced in a highly metastatic lung cancer cell line and was most significantly associated with favorable prognosis in lung cancer patients, could reduce motility and invasion of lung cancer cells in vitro as well as their metastasis in vivo through both hematogenous and lymphogenous routes (60). We previously reported that the re-expression of NKX2-1 in dedifferentiated thyroid cancer cells was induced by histone deacetylase (HDAC) inhibitors (61). Gene expression is regulated by HDAC and histone acetyltransferase (HAT). HAT has been shown to be deregulated or mutated in several cancers (62). Whereas histone acetylation opens the chromatin structure, allowing for the binding of transcription factors, and leads to gene expression, histone deacetylation confers a close chromatin structure and inhibits or decreases gene transcription. Thus, HDAC inhibitors maintain an open chromatin conformation, inducing transcriptional activation. It was also reported that HDAC

inhibitors promoted caspase-mediated apoptosis in thyroid cancer cells (63). Accordingly, exploring factors which effectively induce re-expression of the *NKX2-1* gene would lead to novel approaches to the treatment of dedifferentiated thyroid cancer.

In conclusion, the forced expression of NKX2-1 using adenoviral vectors induced cell death in dedifferentiated thyroid cancer cells not-expressing NKX2-1. In addition, the induction of NKX2-1 expression also caused cell apoptosis and necrosis in those cells. The suppression of *ARG2* and *RGS4* gene expressions resulted in partial inhibition of cell death, apoptosis, and necrosis after the re-expression of NKX2-1 in the dedifferentiated thyroid carcinoma cells. Our study results suggest that ARG2 and RGS4 have a partial role in the suppression of tumor progression. These findings could provide new perspectives on the mechanisms of progression and novel therapeutic approaches of dedifferentiated thyroid carcinoma.

References

1. Fernandez LP, Lopez-Marquez A, Santisteban P. Thyroid transcription factors in development, differentiation and disease. Nat Rev Endocrinol. 2015;11(1):29-42.
2. Kimura S. Thyroid-specific transcription factors and their roles in thyroid cancer. J Thyroid Res. 2011;2011:710213.
3. Tong GX, Yu WM, Beaubier NT, Weeden EM, Hamele-Bena D, Mansukhani MM, et al. Expression of PAX8 in normal and neoplastic renal tissues: an immunohistochemical study. Mod Pathol. 2009;22(9):1218-27.
4. Poleev A, Fickenscher H, Mundlos S, Winterpacht A, Zabel B, Fidler A, et al. PAX8, a human paired box gene: isolation and expression in developing thyroid, kidney and Wilms' tumors. Development. 1992;116(3):611-23.
5. Wiseman W, Michael CW, Roh MH. Diagnostic utility of PAX8 and PAX2 immunohistochemistry in the identification of metastatic Mullerian carcinoma in effusions. Diagn Cytopathol. 2011;39(9):651-6.
6. Riesco-Eizaguirre G, Leoni SG, Mendiola M, Estevez-Cebrero MA, Gallego MI, Redondo A, et al. NIS mediates iodide uptake in the female reproductive tract and is a poor prognostic factor in ovarian cancer. J Clin Endocrinol Metab. 2014;99(7):E1199-208.
7. Barletta JA, Perner S, Iafrate AJ, Yeap BY, Weir BA, Johnson LA, et al. Clinical significance of TTF-1 protein expression and TTF-1 gene amplification in lung adenocarcinoma. J Cell Mol Med. 2009;13(8B):1977-86.
8. Myong NH. Thyroid transcription factor-1 (TTF-1) expression in human lung carcinomas: its prognostic implication and relationship with wxpressions of p53 and Ki-67 proteins. J Korean Med Sci. 2003;18(4):494-500.
9. Kusakabe T, Kawaguchi A, Hoshi N, Kawaguchi R, Hoshi S, Kimura S. Thyroid-specific enhancer-binding protein/NKX2.1 is required for the maintenance of ordered architecture and function of the differentiated thyroid. Mol Endocrinol. 2006;20(8):1796-809.
10. Hoshi S, Hoshi N, Okamoto M, Paiz J, Kusakabe T, Ward JM, et al. Role of NKX2-1 in N-bis(2-hydroxypropyl)-nitrosamine-induced thyroid adenoma in mice. Carcinogenesis. 2009;30(9):1614-9.
11. Kondo T, Ezzat S, Asa SL. Pathogenetic mechanisms in thyroid follicular-cell neoplasia. Nat Rev Cancer. 2006;6(4):292-306.
12. Zhang P, Zuo H, Nakamura Y, Nakamura M, Wakasa T, Kakudo K. Immunohistochemical

analysis of thyroid-specific transcription factors in thyroid tumors. Pathol Int. 2006;56(5):240-5.

13. Fugazzola L, Elisei R, Fuhrer D, Jarzab B, Leboulleux S, Newbold K, et al. 2019 European Thyroid Association Guidelines for the Treatment and Follow-Up of Advanced Radioiodine-Refractory Thyroid Cancer. Eur Thyroid J. 2019;8(5):227-45.
14. Ros P, Rossi DL, Acebron A, Santisteban P. Thyroid-specific gene expression in the multi-step process of thyroid carcinogenesis. Biochimie. 1999;81(4):389-96.
15. Furuya F, Shimura H, Miyazaki A, Taki K, Ohta K, Haraguchi K, et al. Adenovirus-mediated transfer of thyroid transcription factor-1 induces radioiodide organification and retention in thyroid cancer cells. Endocrinology. 2004;145(11):5397-405.
16. Yamaguchi T, Hosono Y, Yanagisawa K, Takahashi T. NKX2-1/TTF-1: an enigmatic oncogene that functions as a double-edged sword for cancer cell survival and progression. Cancer Cell. 2013;23(6):718-23.
17. Shimura H, Suzuki H, Miyazaki A, Furuya F, Ohta K, Haraguchi K, et al. Transcriptional activation of the thyroglobulin promoter directing suicide gene expression by thyroid transcription factor-1 in thyroid cancer cells. Cancer Res. 2001;61(9):3640-6.
18. Ohta K, Pang XP, Berg L, Hershman JM. Growth inhibition of new human thyroid carcinoma cell lines by activation of adenylate cyclase through the beta-adrenergic receptor. J Clin Endocrinol Metab. 1997;82(8):2633-8.
19. Ichijo S, Furuya F, Shimura H, Hayashi Y, Takahashi K, Ohta K, et al. Activation of the RhoB signaling pathway by thyroid hormone receptor beta in thyroid cancer cells. PLoS One. 2014;9(12):e116252.
20. Livak KJ, Schmittgen TD. Analysis of relative gene expression data using real-time quantitative PCR and the 2(-Delta Delta C(T)) Method. Methods. 2001;25(4):402-8.
21. Ibrahimpasic T, Ghossein R, Shah JP, Ganly I. Poorly Differentiated Carcinoma of the Thyroid Gland: Current Status and Future Prospects. Thyroid. 2019;29(3):311-21.
22. Lee DY, Won JK, Lee SH, Park DJ, Jung KC, Sung MW, et al. Changes of Clinicopathologic Characteristics and Survival Outcomes of Anaplastic and Poorly Differentiated Thyroid Carcinoma. Thyroid. 2016;26(3):404-13.
23. Vanden Berghe T, Linkermann A, Jouan-Lanhouet S, Walczak H, Vandenabeele P. Regulated necrosis: the expanding network of non-apoptotic cell death pathways. Nat Rev Mol Cell Biol. 2014;15(2):135-47.

24. Griesing S, Kajino T, Tai MC, Liu Z, Nakatochi M, Shimada Y, et al. Thyroid transcription factor-1-regulated microRNA-532-5p targets KRAS and MKL2 oncogenes and induces apoptosis in lung adenocarcinoma cells. Cancer Sci. 2017;108(7):1394-404.
25. Zu YF, Wang XC, Chen Y, Wang JY, Liu X, Li X, et al. Thyroid transcription factor 1 represses the expression of Ki-67 and induces apoptosis in non-small cell lung cancer. Oncol Rep. 2012;28(5):1544-50.
26. Galluzzi L, Vitale I, Abrams JM, Alnemri ES, Baehrecke EH, Blagosklonny MV, et al. Molecular definitions of cell death subroutines: recommendations of the Nomenclature Committee on Cell Death 2012. Cell Death Differ. 2012;19(1):107-20.
27. Nehs MA, Lin CI, Kozono DE, Whang EE, Cho NL, Zhu K, et al. Necroptosis is a novel mechanism of radiation-induced cell death in anaplastic thyroid and adrenocortical cancers. Surgery. 2011;150(6):1032-9.
28. Lin CY, Chang TW, Hsieh WH, Hung MC, Lin IH, Lai SC, et al. Simultaneous induction of apoptosis and necroptosis by Tanshinone IIA in human hepatocellular carcinoma HepG2 cells. Cell Death Discov. 2016;2:16065.
29. Primon M, Hunter KD, Pandha HS, Morgan R. Kinase Regulation of HOX Transcription Factors. Cancers (Basel). 2019;11(4):508.
30. Elsir T, Smits A, Lindstrom MS, Nister M. Transcription factor PROX1: its role in development and cancer. Cancer Metastasis Rev. 2012;31(3-4):793-805.
31. Caramel J, Ligier M, Puisieux A. Pleiotropic Roles for ZEB1 in Cancer. Cancer Res. 2018;78(1):30-5.
32. Nagel S, Drexler HG. Deregulated NKL Homeobox Genes in B-Cell Lymphoma. Cancers (Basel). 2019;11(12):1874
33. Li H, Meininger CJ, Hawker JR, Jr., Haynes TE, Kepka-Lenhart D, Mistry SK, et al. Regulatory role of arginase I and II in nitric oxide, polyamine, and proline syntheses in endothelial cells. Am J Physiol Endocrinol Metab. 2001;280(1):E75-82.
34. Patil MD, Bhaumik J, Babykutty S, Banerjee UC, Fukumura D. Arginine dependence of tumor cells: targeting a chink in cancer's armor. Oncogene. 2016;35(38):4957-72.
35. Sousa MS, Latini FR, Monteiro HP, Cerutti JM. Arginase 2 and nitric oxide synthase: Pathways associated with the pathogenesis of thyroid tumors. Free Radic Biol Med. 2010;49(6):997-1007.
36. Singh R, Pervin S, Karimi A, Cederbaum S, Chaudhuri G. Arginase activity in human breast

cancer cell lines: N(omega)-hydroxy-L-arginine selectively inhibits cell proliferation and induces apoptosis in MDA-MB-468 cells. Cancer Res. 2000;60(12):3305-12.

37. Mumenthaler SM, Rozengurt N, Livesay JC, Sabaghian A, Cederbaum SD, Grody WW. Disruption of arginase II alters prostate tumor formation in TRAMP mice. Prostate. 2008;68(14):1561-9.
38. Squires KE, Montanez-Miranda C, Pandya RR, Torres MP, Hepler JR. Genetic Analysis of Rare Human Variants of Regulators of G Protein Signaling Proteins and Their Role in Human Physiology and Disease. Pharmacol Rev. 2018;70(3):446-74.
39. Mirnics K, Middleton FA, Stanwood GD, Lewis DA, Levitt P. Disease-specific changes in regulator of G-protein signaling 4 (RGS4) expression in schizophrenia. Mol Psychiatry. 2001;6(3):293-301.
40. Emilsson L, Saetre P, Jazin E. Low mRNA levels of RGS4 splice variants in Alzheimer's disease: association between a rare haplotype and decreased mRNA expression. Synapse. 2006;59(3):173-6.
41. Ho AM, MacKay RK, Dodd PR, Lewohl JM. Association of polymorphisms in RGS4 and expression of RGS transcripts in the brains of human alcoholics. Brain Res. 2010;1340:1-9.
42. Xie Y, Wolff DW, Wei T, Wang B, Deng C, Kirui JK, et al. Breast cancer migration and invasion depend on proteasome degradation of regulator of G-protein signaling 4. Cancer Res. 2009;69(14):5743-51.
43. Park HJ, Kim SH, Moon DO. Growth inhibition of human breast carcinoma cells by overexpression of regulator of G-protein signaling 4. Oncol Lett. 2017;13(6):4357-63.
44. Lee EK, Ye Y, Kamat AM, Wu X. Genetic variations in regulator of G-protein signaling (RGS) confer risk of bladder cancer. Cancer. 2013;119(9):1643-51.
45. Adams LD, Geary RL, Li J, Rossini A, Schwartz SM. Expression profiling identifies smooth muscle cell diversity within human intima and plaque fibrous cap: loss of RGS5 distinguishes the cap. Arterioscler Thromb Vasc Biol. 2006;26(2):319-25.
46. Hamzah J, Jugold M, Kiessling F, Rigby P, Manzur M, Marti HH, et al. Vascular normalization in Rgs5-deficient tumours promotes immune destruction. Nature. 2008;453(7193):410-4.
47. Hernandez CP, Morrow K, Lopez-Barcons LA, Zabaleta J, Sierra R, Velasco C, et al. Pegylated arginase I: a potential therapeutic approach in T-ALL. Blood. 2010;115(25):5214-21.
48. Lam TL, Wong GK, Chow HY, Chong HC, Chow TL, Kwok SY, et al. Recombinant human arginase inhibits the in vitro and in vivo proliferation of human melanoma by inducing cell

cycle arrest and apoptosis. Pigment Cell Melanoma Res. 2011;24(2):366-76.

49. Khoury O, Ghazale N, Stone E, El-Sibai M, Frankel AE, Abi-Habib RJ. Human recombinant arginase I (Co)-PEG5000 [HuArgI (Co)-PEG5000]-induced arginine depletion is selectively cytotoxic to human glioblastoma cells. J Neurooncol. 2015;122(1):75-85.
50. Wang Y, Zhao P, Qian D, Hu M, Zhang L, Shi H, et al. MicroRNA-613 is downregulated in HCMV-positive glioblastoma and inhibits tumour progression by targeting arginase-2. Tumour Biol. 2017;39(7):1010428317712512.
51. Xue X, Wang L, Meng X, Jiao J, Dang N. Regulator of G protein signaling 4 inhibits human melanoma cells proliferation and invasion through the PI3K/AKT signaling pathway. Oncotarget. 2017;8(45):78530-44.
52. Xiao D, Gao HX. Mechanism of miR-107-targeting of regulator of G-protein signaling 4 in hepatocellular carcinoma. Oncol Lett. 2019;18(5):5145-54.
53. He Z, Yu L, Luo S, Li Q, Huang S, An Y. RGS4 Regulates Proliferation And Apoptosis Of NSCLC Cells Via microRNA-16 And Brain-Derived Neurotrophic Factor. Onco Targets Ther. 2019;12:8701-14.
54. Ji L, Fan X, Zhou F, Gu J, Deng X. lncRNA RPL34-AS1 inhibits cell proliferation and invasion while promoting apoptosis by competitively binding miR-3663-3p/RGS4 in papillary thyroid cancer. J Cell Physiol. 2020;235(4):3669-78.
55. Altman MK, Nguyen DT, Patel SB, Fambrough JM, Beedle AM, Hardman WJ, et al. Regulator of G-Protein Signaling 5 Reduces HeyA8 Ovarian Cancer Cell Proliferation and Extends Survival in a Murine Tumor Model. Biochem Res Int. 2012;2012:518437.
56. Xu Z, Zuo Y, Wang J, Yu Z, Peng F, Chen Y, et al. Overexpression of the regulator of G-protein signaling 5 reduces the survival rate and enhances the radiation response of human lung cancer cells. Oncol Rep. 2015;33(6):2899-907.
57. Abate-Shen C. Deregulated homeobox gene expression in cancer: cause or consequence? Nat Rev Cancer. 2002;2(10):777-85.
58. Phelps CA, Lai SC, Mu D. Roles of Thyroid Transcription Factor 1 in Lung Cancer Biology. Vitam Horm. 2018;106:517-44.
59. Li CM, Gocheva V, Oudin MJ, Bhutkar A, Wang SY, Date SR, et al. Foxa2 and Cdx2 cooperate with Nkx2-1 to inhibit lung adenocarcinoma metastasis. Genes Dev. 2015;29(17):1850-62.
60. Tomida S, Yanagisawa K, Koshikawa K, Yatabe Y, Mitsudomi T, Osada H, et al. Identification of a metastasis signature and the DLX4 homeobox protein as a regulator of metastasis by

combined transcriptome approach. Oncogene. 2007;26(31):4600-8.

61. Furuya F, Shimura H, Suzuki H, Taki K, Ohta K, Haraguchi K, et al. Histone deacetylase inhibitors restore radioiodide uptake and retention in poorly differentiated and anaplastic thyroid cancer cells by expression of the sodium/iodide symporter thyroperoxidase and thyroglobulin. Endocrinology. 2004;145(6):2865-75.
62. San Jose-Eneriz E, Gimenez-Camino N, Agirre X, Prosper F. HDAC Inhibitors in Acute Myeloid Leukemia. Cancers (Basel). 2019;11(11):1794
63. Mitsiades CS, Poulaki V, McMullan C, Negri J, Fanourakis G, Goudopoulou A, et al. Novel histone deacetylase inhibitors in the treatment of thyroid cancer. Clin Cancer Res. 2005;11(10):3958-65.

Acknowledgments

I would like to express my greatest appreciation to Professor Hiroki Shimura at Department of Laboratory Medicine in Fukushima Medical University for his thoughtful guidance. I would also like to give special thanks to Dr. Katsumi Taki at Fujiyoshida Municipal Medical Center and Dr. Fumihiko Furuya at University of Yamanashi for their valuable advice and encouragement. I would like to thank Chisato Takahashi for her technical assistance, Daiki Tanno for supporting the data analyses, and Junko Suga for her helpful advice on the experiments. This work was supported by JSPS KAKENHI Grant Number JP16K08971 and JP17K15779.